J/ψ pair production in hadronic collisions

Bing-An Li* and Keh-Fei Liu

Department of Physics and Astronomy, University of Kentucky, Lexington, Kentucky 40506

(Received 27 June 1983; revised manuscript received 14 October 1983)

Resonance productions of J/ψ pairs in πp and pp collisions are calculated in a Drell-Yan-type mechanism with gluon fusion via the color vector-dominance model. The calculated cross sections and the longitudinal-momentum distributions are consistent with the $\pi p \rightarrow JJX$ data at $p_L = 150$ and 280 GeV/c. They are 20–30 times larger than the perturbative QCD results for $q\bar{q}/gg \rightarrow JJ$. Calculations for the resonance productions of $J\omega$, $D^*\bar{D}^*$, $J\phi$, $F^*\bar{F}^*$, $\Upsilon\Upsilon$, $\Upsilon\omega$, $B^*\bar{B}^*$, $\Upsilon\phi$, $B_s^*\bar{B}_s^*$, ΥJ, and $B_c^*\bar{B}_c^*$ in πp and pp collisions are also presented.

Evidence for J/ψ pair production in $\pi^- N$ collisions at 150 and 280 GeV/c has been reported by the NA3 collaboration at CERN.[1] The observed $\pi^- N \rightarrow JJX$ events reveal the following salient features.

(1) There is a strong correlation between the two J/ψ mesons. The mean value of the individual J/ψ transverse momentum is 1.5 ± 0.1 GeV/c, whereas the average transverse momentum of the J/ψ pair is only 0.9 ± 0.1 GeV/c for a 280-GeV/c beam, which is much lower than that of the uncorrelated J/ψ pair from a Monte Carlo simulation at 1.7 GeV/c.

(2) The invariant mass of the J/ψ pair spreads from 6.5 to 8.5 GeV, which is somewhat higher than the most probable value of the spectrum obtained from Monte Carlo uncorrelated pairs.

(3) The longitudinal-momentum distribution indicates that one J/ψ is fast, the other is slow.

(4) The cross sections are 18 ± 8 pb at 150 GeV/c and 30 ± 10 pb at 280 GeV/c.

Several production mechanisms[2-5] have been proposed to describe the results. A perturbative QCD calculation of $q\bar{q}$ annihilation has been carried out in Refs. 2 and 4 to $O(\alpha_s^4)$. With $\alpha_s = 0.32$, the calculated cross sections are ~ 5 times smaller than the experimental values.[2] In Ref. 3, it was proposed that the J/ψ pair originates from $B\bar{B}$ production with subsequent inclusive B decay to J/ψ. A systematic study of J/ψ pair production via $q\bar{q}$ annihilation, gluon fusion, and B-meson decay in perturbative QCD has been done by Humpert and Méry.[5] It was found that J/ψ pair production via B-meson decay is negligibly small and the direct J/ψ production via gg and $q\bar{q}$ annihilation at $\alpha_s = 0.3$ are 3–5 times smaller than the experimental values.

In this paper, we shall calculate the J/ψ pair production in hadronic collisions based on a Drell-Yan-type mechanism where two gluons fuse via "color vector-dominance model (VDM)" to a 2^{++} $c^2\bar{c}^2$ state, which decays subsequently into J/ψ pairs. This mechanism, depicted in Fig. 1, has been used to calculate the 2^{++} $\phi\phi$ resonance (2160 MeV) production in the pp reaction at $p_L = 400$ GeV/c and the πp reaction at $p_L = 100$ GeV/c.[6] The theoretical $\phi\phi$ production cross sections agree with the experimental data.[7] The JJ production calculation in this paper is motivated by the observation that the invariant mass of the J/ψ pair lies somewhat higher than that of the uncorrelated pairs and has roughly two peaks (one centers around 7 GeV, the other around 8 GeV) which resemble the two $\phi\phi$ resonance peaks observed at 2160 and 2310 MeV.[8] Furthermore, 2^{++} $Q^2\bar{Q}^2$ states which decay to vector-meson pairs predominantly are expected to be produced copiously in hadronic collisions. These 2^{++} $Q^2\bar{Q}^2$ are believed to have been observed in $\gamma\gamma$ reactions[9] [i.e., $\gamma\gamma \rightarrow \rho^0\rho^0$ (Ref. 10)], radiative decay of J/ψ [i.e., $J/\psi \rightarrow \gamma\rho^0\rho^0$ (Ref. 11)], and hadronic collisions[6] [i.e., $\pi p(pp) \rightarrow \phi\phi X$ (Ref. 7)].

Upon interpreting the J/ψ pair to be produced via the 2^{++} $c^2\bar{c}^2$ state, we can calculate its production cross section in the parton model as depicted in Fig. 1. The production cross section can be written as

$$\sigma(h_1 + h_2 \rightarrow V_1 + V_2 + \cdots) = \int_{x_{1\min}}^1 dx_1 \int_{x_{2\min}}^1 dx_2 [G_{g_1}^{h_1}(x_1)G_{g_2}^{h_2}(x_2) + G_{g_2}^{h_1}(x_1)G_{g_1}^{h_2}(x_2)]\sigma(g_1 + g_2 \rightarrow Q^2\bar{Q}^2 \rightarrow V_1V_2) ,$$

where

$$x_{2\min} = \frac{(m_1 + m_2)^2}{x_1 s}, \quad x_{1\min} = \frac{(m_1 + m_2)^2}{s} , \quad (1)$$

$\sqrt{s}$ is the total energy in the center-of-mass frame, and $G_g^h(x)$ is the gluon distribution function inside the hadron h. The gluon distribution function of the π meson is taken from the J/ψ production experiment[12]

$$G_g^\pi(x) = (1-x)^{1.9}/x , \quad (2)$$

and we take the gluon distribution function of the proton to be[13]

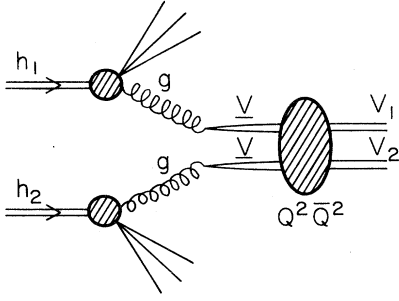$$G_g^p(x) = 2.62(1 + 3.5x)(1-x)^{5.9}/x . \quad (3)$$

FIG. 1. Drell-Yan-type mechanism for the resonance production of two vector mesons. $\underline{V}$ denotes a color-octet vector $Q\overline{Q}$ pair; V_1 and V_2 denote the two vector mesons. The intermediate states are four-quark states.

To evaluate the cross section for the process

$$g + g \rightarrow Q^2\overline{Q}^2 \rightarrow V_1 + V_2 , \qquad (4)$$

we have assumed[6] a mechanism analogous to the VDM where the gluons couple to the $Q\overline{Q}$ pairs in the color-octet vector representation, which in turn coupled to the $\underline{V} \cdot \underline{V}$ (color-octet-vector—color-octet-vector) part of the $Q^2\overline{Q}^2$ state. This is done in parallel to the calculation[9] of the process

$$\gamma\gamma \rightarrow Q^2\overline{Q}^2 \rightarrow V_1 + V_2 , \qquad (5)$$

where the photons are coupled to neutral vector mesons which in turn couple to the $\underline{VV}$ (color-singlet-vector—color-singlet-vector) part of the $Q^2\overline{Q}^2$ state. The color-VDM constant between the gluon and the color-octet vector $Q\overline{Q}$ is related[6] to the VDM constant in the form

$$\frac{4\pi}{f_{\underline{V}}^2} = \frac{1}{6} \frac{(T_r \phi_V)^2}{(T_r Q\phi_V)^2} \frac{m_V^3}{m_{\underline{V}}^3} \frac{4\pi}{f_V^2} , \qquad (6)$$

where ϕ_V is the flavor wave function of the vector meson, Q is the charge operator, and $m_{\underline{V}}$ is the "effective" mass of the $Q\overline{Q}$ pair in the color-octet vector representation which we take to be half of the $Q^2\overline{Q}^2$ mass. These color-VDM constants are thus determined to be

$$\frac{4\pi}{f_{\underline{\omega}}^2} = 0.273 , \quad \frac{4\pi}{f_{\underline{\phi}}^2} = 0.087,$$

$$\frac{4\pi}{f_{\underline{J}}^2} = 0.02 , \quad \frac{4\pi}{f_{\underline{\Upsilon}}^2} = 0.011 . \qquad (7)$$

We do not expect these values to be very accurate. Even in the VDM there are appreciable differences between the values of $4\pi/f_V^2$ determined from the photon production and the electromagnetic annihilation. Since the $\phi\phi$ production cross sections are well reproduced with $4\pi/f_\phi^2 = 0.087$,[6] we believe these color-VDM constants are useful in estimating the $h_1 + h_2 \rightarrow V_1 + V_2 + \cdots$ cross sections and in testing the picture of $Q^2\overline{Q}^2$ productions.

The cross section $\sigma(gg \rightarrow Q^2\overline{Q}^2(2^{++}) \rightarrow VV)$ is written as

$$\sigma(g_1 + g_2 \rightarrow Q^2\overline{Q}^2 \rightarrow V_1 + V_2) = \frac{1}{64} \frac{p}{128\pi W} \frac{7}{3} \left[1 + \frac{p^2}{3} \left[\frac{1}{m_1^2} + \frac{1}{m_2^2} \right] + \frac{2}{15} \frac{p^4}{m_1^2 m_2^2} \right]$$

$$\times \sum_{\alpha\beta} \left| \sum_j \frac{a_{V_1 V_2}^j b_{\alpha\beta}^j}{W - M_j + (i/2)\Gamma_j(W)} \right|^2 , \qquad (8)$$

where m_1 and m_2 are the masses of the vector mesons V_1 and V_2, respectively, W is the cm energy of the two gluons, p is the momentum of the vector meson in the c.m. frame, and M_j and Γ_j are the mass and width of the jth four-quark state. $a_{V_1 V_2}^j$ is the decay constant of the jth four-quark state decaying to vector mesons V_1 and V_2 and $b_{\alpha\beta}^j$ is the coupling constant between the jth four-quark state and the two gluons via two color-octet vector $Q\overline{Q}$ pairs. Both a^j and b^j depend on the color and flavor contents of the corresponding four-quark state.[6,9]

For J/ψ pair production, the structure of the 2^{++} $c^2\overline{c}^2$ state yields the decay constant a_{JJ} to be

$$a_{JJ} = \frac{1}{\sqrt{3}} a , \qquad (9)$$

and the $b_{\alpha\beta}$ to be

$$b_{\alpha\beta}(JJ) = (\tfrac{2}{3})^{1/2} \frac{4\pi}{f_{\underline{J}}^2} \alpha_s a \frac{1}{\sqrt{8}} \delta_{\alpha\beta} , \qquad (10)$$

where a has been determined to be $\cong \sqrt{30}$ by fitting the width of the first peak in the J/ψ-pair events around 7 GeV to be ~ 0.8 GeV. This is somewhat smaller than the value we used to fit the $\gamma\gamma \rightarrow \rho^0\rho^0$ width which is $\sim\sqrt{50}$.[9]
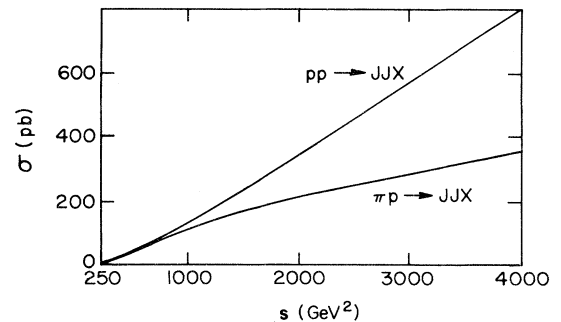

FIG. 2. The calculated cross sections for the processes $\pi p \rightarrow JJX$ and $pp \rightarrow JJX$ as a function of s.

Taking into account the fact that the two processes occur at fairly different energies, i.e., $\gamma\gamma\rightarrow\rho^0\rho^0$ is at ~1.65 GeV yet $\pi p\rightarrow JJX$ is at ~7 GeV, these two values of a indicate that it is fairly constant. α_s is the running coupling constant which we have taken to be

$$\alpha_s(M_j)=\frac{4\pi}{\beta_0\ln(M_j^2/\Lambda^2)} \ , \tag{11}$$

where $\beta_0=11-\frac{2}{3}f$, with f being the flavor number, which is taken to be 4 for these $Q^2\bar{Q}^2$ states which do not involve b quarks and 5 for those which do. M_j is the mass of the jth four-quark state. With Λ being 0.1 GeV, we get $\alpha_s=0.18$ for J/ψ pair production at ~7 GeV.

Using those parameters in Eqs. (7), (9), (10), and (11), we obtain from Eqs. (8) and (1) that the cross sections for $\pi^-p\rightarrow JJX$ to be 39.3 pb at $p_L=280$ GeV/c and 9.3 pb at $p_L=150$ GeV/c. They are at one standard deviation from the experimental cross sections of 30 ± 10 pb and 18 ± 8 pb at these energies.[1] The results for $\pi^-p\rightarrow JJX$ and $pp\rightarrow JJX$ at different energies are plotted in Fig. 2. The increase of the production cross sections are attributed to the $1/x$ behavior of the gluon distribution function as x approaches zero. The fact that pp cross sections are larger than those of the πp collisions is due to the fact that the gluon distribution function inside the proton is proportional to $(1-x)^{5.9}$ as opposed to $(1-x)^{1.9}$ in the π meson. At collider energies, $\sigma(pp(p\bar{p})\rightarrow JJX)$ is predicted to be 3.4 nb at $\sqrt{s}=400$ GeV and 3.8 nb at $\sqrt{s}=540$ GeV.

To compare with the perturbative QCD calculations,[2,5] we note that the α_s used in those calculations are $\alpha_s\cong0.3$ which are larger than our value at $\alpha_s=0.18$. After correcting for this difference, we find that the perturbative QCD calculations are $20-30$ times smaller than our results. This order-of-magnitude difference, we believe, is ascribed mainly to the fact that in our picture the J/ψ
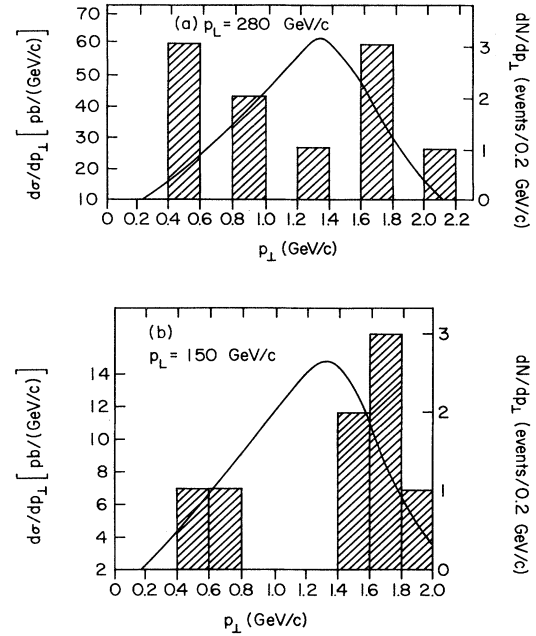

FIG. 3. The calculated transverse differential cross section $d\sigma/dp_\perp$ for a single J/ψ in $\pi p\rightarrow JJX$ at (a) $p_L=280$ GeV/c and (b) $p_L=150$ GeV/c, together with the experimental data. The scales for the experimental events are to the right.

pair production is enhanced by the 2^{++} $cc\bar{c}\bar{c}$ resonance.

The experimental features on the longitudinal-momentum and transverse momentum distribution can also be understood in terms of this resonance-production mechanism. The transverse differential cross section $d\sigma/dp_\perp$ for a single J/ψ is given as

$$\frac{d\sigma}{dp_\perp}=\frac{2}{s}\int_{W_{\min}^2}^s dW^2\int_0^1 dz\frac{p_\perp}{k}\frac{1}{(k^2-p_\perp^2)^{1/2}}\frac{1}{(z^2+W^2/p_L^2)^{1/2}}G_{g_1}^{h_1}(x_1)G_{g_2}^{h_2}(x_2)$$

$$\times\frac{d}{d\cos\theta}\sigma(q_1+q_2\rightarrow Q^2\bar{Q}^2\rightarrow V_1+V_2) \ , \tag{12}$$

where

$$\cos\theta=(1-p_\perp^2/k^2)^{1/2}, \quad k^2=\frac{1}{4W^2}(W^2+m_1^2-m_2^2)^2-m_1^2 \ ,$$

$$W_{\min}^2=[(m_1^2+p_\perp^2)^{1/2}+(m_2^2+p_\perp^2)^{1/2}]^2 \ , \tag{13}$$

$$x_1=\frac{y}{2}+\frac{1}{2}\left[y^2+\frac{4W^2}{s}\right]^{1/2}, \quad x_2=-\frac{y}{2}+\frac{1}{2}\left[y^2+\frac{4W^2}{s}\right]^{1/2}, \quad y=\frac{2p_L}{\sqrt{s}}\frac{z-v(z^2+W^2/p_L^2)^{1/2}}{(1-v^2)^{1/2}}, \quad v=\frac{p_L}{M_N+E_L} \ ,$$

$$\frac{d}{d\cos\theta}\sigma(g_1+g_2\rightarrow Q^2\bar{Q}^2\rightarrow V_1+V_2)=\frac{1}{64}\frac{k}{128\pi W}\left[\frac{7}{3}+k^2\left[\frac{1}{m_1^2}+\frac{1}{m_2^2}\right](\tfrac{19}{18}-\tfrac{5}{6}\cos^2\theta)\right.$$

$$\left.+\frac{k^4}{m_1^2m_2^2}(\tfrac{5}{9}-\tfrac{4}{3}\cos^2\theta+\cos^4\theta)\right]\sum_{\alpha\beta}\left|\sum_j\frac{a_{V_1V_2}^j b_{\alpha\beta}^j}{W-M_j+(i/2)\Gamma_j(W)}\right|^2 \ . \tag{14}$$
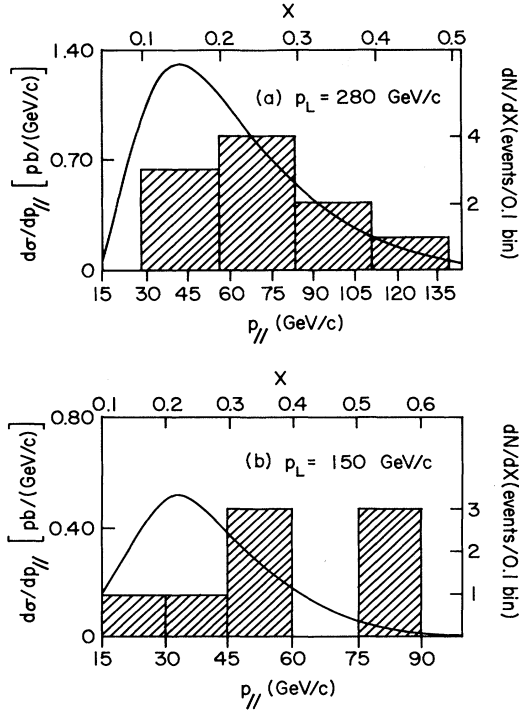
FIG. 4. The calculated longitudinal differential cross section $d\sigma/dp_{\parallel}$ for a single J/ψ in $\pi p \to JJX$ at (a) $p_L = 280$ GeV/c and (b) $p_L = 150$ GeV/c, with experimental data. The scales for the experimental events are to the right.

FIG. 5. The calculated longitudinal differential cross section $d\sigma/dp_{\parallel}^{12}$ for the J/ψ pair in $\pi p \to JJX$ at (a) $p_L = 280$ GeV/c and (b) $p_L = 150$ GeV/c, with experimental data. The scales for the experimental events are to the right of the figure.

For the 2^{++} $c^2\bar{c}^2$ four-quark state we have

$$\Gamma(W) = \frac{a^2 k}{24\pi} \left[1 + \frac{2k^2}{3m_J^2} + \frac{2k^4}{15m_J^4} \right] . \quad (15)$$

The results for $\pi p \to JJX$ at $p_L = 280$ and 150 GeV/c are plotted in Figs. 3(a) and 3(b) together with the experimental distribution for events around 7 GeV. We find that while the calculated $\langle p_\perp \rangle$'s are comparable to the experimental values $[\langle p_\perp \rangle = 1.2 \ (1.18)$ GeV/c at $p_L = 280 \ (150)$ GeV/c versus the experimental value of 1.22 (1.37) GeV/c], the theoretical distributions appear to be somewhat narrower than the corresponding experimental distri-
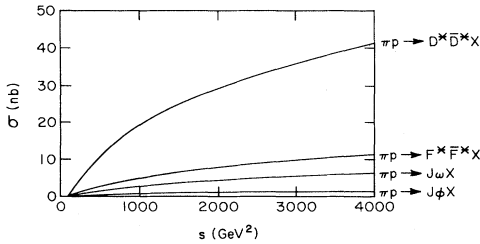
butions. We interpret this "broadening" as due to the transverse momentum of the gluon whose distribution should be folded in to obtain a wider distribution for a single J/ψ. By the same token, the experimental average transverse momentum of 0.9±0.1 GeV/c for the J/ψ pair at $p_L = 280$ GeV/c is interpreted as coming from the two gluons. Since the two J/ψ mesons come out back to back in the center-of-mass frame of the two gluons, the resonance itself does not contribute to the pair transverse momentum. This puts the average transverse momentum of the gluon to be $\sim 400 - 500$ MeV which is comparable to the recent finding of ~ 500 MeV in the jet analysis.[14]

The longitudinal differential cross section for a single J/ψ in the laboratory frame is

FIG. 6. The calculated cross sections for the resonance production of $D^*\bar{D}^*$, $F^*\bar{F}^*$, $J\omega$, and $J\phi$ in πp collisions as a function of s.
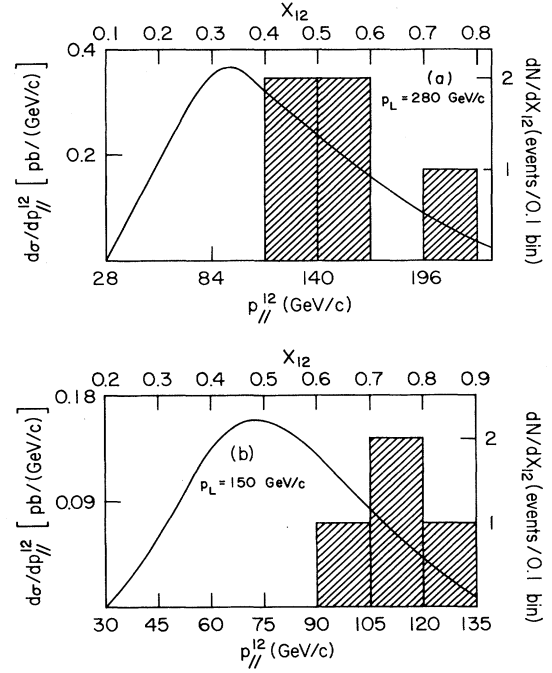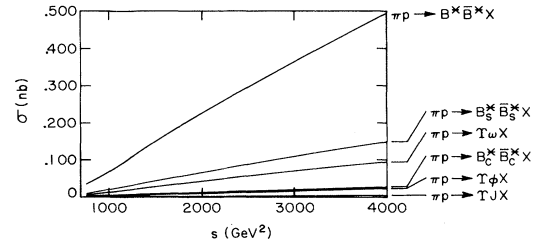

FIG. 7. The calculated cross sections for the resonance production of $B^*\bar{B}^*$, $B_s^*\bar{B}_s^*$, $B_c^*\bar{B}_c^*$, $\Upsilon\omega$, $\Upsilon\phi$, and ΥJ in πp collisions as a function of s.

TABLE I. Parameters used in Eq. (8) to calculate the cross sections for vector-meson pair production. (+) and (−) denote two degenerate 2^{++} $Q^2\bar{Q}^2$ states. Except in the case of JJ, we take $4\pi/f_J^2 = 0.03$, due to the fact that the 2^{++} $Q^2\bar{Q}^2$ are expected to lie not far above the threshold. α_s is determined from Eq. (11).

V_1V_2	$a^j_{V_1V_2}/a$	$b^j_{\alpha\beta}\Big/\alpha_s\dfrac{a}{\sqrt{8}}\delta_{\alpha\beta}$	M_j (GeV)	α_s	m_1
JJ	$1/\sqrt{3}$	$\left[\dfrac{2}{3}\right]^{1/2}\dfrac{4\pi}{f_J^2}$	7.0	0.18	3.10
$J\omega^{(+)}$	$1/\sqrt{6}$	$\dfrac{-1}{\sqrt{3}}\dfrac{4\pi}{f_J f_\omega}$	4.05	0.2	
$J\omega^{(-)}$	$1/\sqrt{12}$	$\left[\dfrac{2}{3}\right]^{1/2}\dfrac{4\pi}{f_J f_\omega}$	4.05	0.2	
$D^*\bar{D}^{*(+)}$	$-1/\sqrt{6}$	$\dfrac{-1}{\sqrt{3}}\dfrac{4\pi}{f_J f_\omega}$	4.05	0.2	2.01
$D^*\bar{D}^{*(-)}$	$1/\sqrt{12}$	$\left[\dfrac{2}{3}\right]^{1/2}\dfrac{4\pi}{f_J f_\omega}$	4.05	0.2	
$J\phi^{(+)}$	$-1/\sqrt{6}$	$\dfrac{-1}{\sqrt{3}}\dfrac{4\pi}{f_J f_\phi}$	4.40	0.2	
$J\phi^{(-)}$	$1/\sqrt{12}$	$\left[\dfrac{2}{3}\right]^{1/2}\dfrac{4\pi}{f_J f_\phi}$	4.40	0.2	
$F^*\bar{F}^{*(+)}$	$-1/\sqrt{6}$	$\dfrac{-1}{\sqrt{3}}\dfrac{4\pi}{f_J f_\phi}$	4.40	0.2	2.16
$F^*\bar{F}^{*(-)}$	$1/\sqrt{12}$	$\left[\dfrac{2}{3}\right]^{1/2}\dfrac{4\pi}{f_J f_\phi}$	4.40	0.2	
$\Upsilon\Upsilon$	$1/\sqrt{3}$	$\left[\dfrac{2}{3}\right]^{1/2}\dfrac{4\pi}{f_\Upsilon^2}$	20	0.16	9.46
$\Upsilon\omega^{(+)}$	$1/\sqrt{6}$	$\dfrac{-1}{\sqrt{3}}\dfrac{4\pi}{f_\Upsilon f_\omega}$	10.8	0.175	
$\Upsilon\omega^{(-)}$	$1/\sqrt{12}$	$\left[\dfrac{2}{3}\right]^{1/2}\dfrac{4\pi}{f_\Upsilon f_\omega}$	10.8	0.175	
$B^*\bar{B}^{*(+)}$	$-1/\sqrt{6}$	$\dfrac{-1}{\sqrt{3}}\dfrac{4\pi}{f_\Upsilon f_\omega}$	10.8	0.175	5.35
$B^*\bar{B}^{*(-)}$	$1/\sqrt{12}$	$\left[\dfrac{2}{3}\right]^{1/2}\dfrac{4\pi}{f_\Upsilon f_\omega}$	10.8	0.175	
$\Upsilon\phi^{(+)}$	$1/\sqrt{6}$	$\dfrac{-1}{\sqrt{3}}\dfrac{4\pi}{f_\Upsilon f_\phi}$	11.1	0.174	
$\Upsilon\phi^{(-)}$	$1/\sqrt{12}$	$\left[\dfrac{2}{3}\right]^{1/2}\dfrac{4\pi}{f_\Upsilon f_\phi}$	11.1	0.174	
$B_s^*\bar{B}_s^{*(+)}$	$-1/\sqrt{6}$	$\dfrac{-1}{\sqrt{3}}\dfrac{4\pi}{f_\Upsilon f_\phi}$	11.1	0.174	5.47

TABLE I. (Continued.)

$V_1 V_2$	$a_{V_1 V_2}^j/a$	$b_{\alpha\beta}^j \left/ \alpha_s \dfrac{a}{\sqrt{8}} \delta_{\alpha\beta}\right.$	M_j (GeV)	α_s	m_1
$B_s^* B_s^{*(-)}$	$1/\sqrt{12}$	$\left[\dfrac{2}{3}\right]^{1/2} \dfrac{4\pi}{f_\chi f_\phi}$	11.1	0.174	
$\Upsilon J^{(+)}$	$1/\sqrt{6}$	$\dfrac{-1}{\sqrt{3}} \dfrac{4\pi}{f_\chi f_J}$	13.5	0.167	
$\Upsilon J^{(-)}$	$1/\sqrt{12}$	$\left[\dfrac{2}{3}\right]^{1/2} \dfrac{4\pi}{f_\chi f_J}$	13.5	0.167	
$B_c^* \bar{B}_c^{*(+)}$	$-1/\sqrt{6}$	$\dfrac{-1}{\sqrt{3}} \dfrac{4\pi}{f_\chi f_J}$	13.5	0.167	6.60
$B_c^* \bar{B}_c^{*(-)}$	$1/\sqrt{12}$	$\left[\dfrac{2}{3}\right]^{1/2} \dfrac{4\pi}{f_\chi f_J}$	13.5	0.167	

$$\frac{d\sigma}{dp_{\|}} = \frac{1}{s} \int_{W_{min}}^{s} 2 dW^2 \int dz \frac{2(1-v_F^2)^{1/2}}{(z^2+W^2/p_L^2)^{1/2}} G_{g_1}^{h_1}(x_1) G_{g_2}^{h_2}(x_2) \frac{1}{k} \frac{d\sigma}{d\cos\theta}(g_1+g_2\to Q^2\bar{Q}^2\to V_1+V_2) , \tag{16}$$

where

$$v_F = \frac{p_F}{E_F}, \quad p_F = zp_L, \quad E_F^2 = p_F^2 + W^2 , \tag{17}$$

p_F and E_F are the momentum and energy of the vector-meson pair,

$$k\cos\theta = \frac{W}{E_F}(p_{\|} - \tfrac{1}{2}zp_L) , \tag{18}$$

and the limits of the variable z are determined by

$$-1 \le \frac{W}{kE_F}(p_{\|} - \tfrac{1}{2}zp_L) \le 1 . \tag{19}$$

Since $d\sigma/dk_{\|}$ is almost symmetric with respect to $k_{\|}$ in the c.m. frame of the hadrons, there will be one fast J/ψ and one slow J/ψ in the laboratory frame in agreement with the experimental observation. We plot $d\sigma/dp_{\|}$ for a single J/ψ in $\pi p \to JJX$ at $p_L = 280$ and 150 GeV/c in Fig. 4 and compare with the experimental data from events around 7 GeV. We find that the shape of the theoretical-differential cross section $d\sigma/dp_{\|}$ agrees qualitatively with the experimental data for $\pi p \to JJX$ at $p_L = 280$ GeV/c. In the case of $p_L = 150$ GeV/c, the calculated results appear to peak on the low side of the experimental distribution. Similarly, the longitudinal differential cross section for the J/ψ pair in the laboratory frame is calculated according to

$$\frac{d\sigma}{dp_{\|}^{12}} = \frac{1}{sp_L} \int_{4M_j^2}^{s} dW^2 \frac{2}{(z^2+W^2/p_L^2)^{1/2}} G_{g_1}^{h_1}(x_1) G_{g_2}^{h_2}(x_2) \sigma(g_1+g_2\to Q^2\bar{Q}^2\to V_1+V_2) , \tag{20}$$
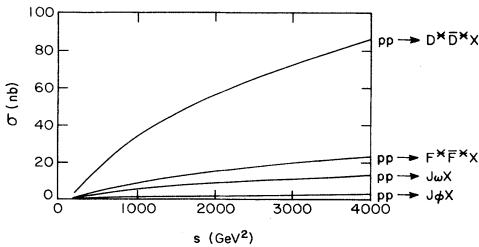

FIG. 8. The calculated cross sections for the resonance production of $D^*\bar{D}^*$, $J\omega$, $F^*\bar{F}^*$, and $J\phi$ in pp collisions as a function of s.
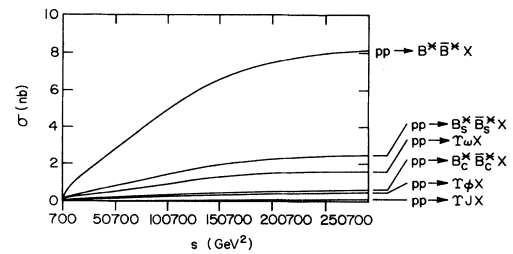
FIG. 9. The calculated cross sections for the resonance production of $B^*\bar{B}^*$, $\Upsilon\omega$, $B_s^*\bar{B}_s^*$, $\Upsilon\phi$, $B_c^*\bar{B}_c^*$, and ΥJ in pp collisions as a function of s.

where z, as in Eq. (13), is the ratio of the J/ψ pair momentum $p_{||}^{12}$ to the laboratory momentum p_L, i.e., $z = p_{||}^{12}/p_L$. The calculated $d\sigma/dp_{||}^{12}$ at $p_L = 280$ and 150 GeV/c are plotted in Figs. 5(a) and 5(b) together with the experimental results from events around 7 GeV. The calculated distributions appear to be peaked lower in $p_{||}^{12}$ than those of the corresponding data. Varying the power of the $(1-x)$ terms in the gluon distribution functions in Eqs. (2) and (3) will improve the agreement between theory and experiment. More data are needed to help settle this difference. Other than the events around 8 GeV, which we believe are attributed to the D-wave JJ resonance in analogy with the D-wave $\phi\phi$ resonance at 2310 MeV, we find that overall our production mechanism can account for the essential features of the JJ events.

Using the same production mechanism, we can predict the production cross sections for vector-meson pairs involving heavy-quark flavors. The parameters used for various channels are tabulated in Table I. The total production cross sections in πp and pp collisions are plotted in Figs. 6—9. Again, the cross sections in general grow with the energy due to the small-x behavior of the gluon distribution functions in Eqs. (2) and (3). The cross sections for the $\Upsilon\Upsilon$ production at $p_L = 280$ and 150 GeV/c are very small ($\sim 10^{-3}$ pb); they reach 62 (81) pb for the pp or $p\bar{p}$ collision at $\sqrt{s} = 400$ (540) GeV.

In summary, we find that the resonance-production mechanism which we used to calculate the $\phi\phi$ production in hadronic collisions can account for the essential features of the J/ψ-pair production events around 7 GeV in $\pi p \rightarrow JJX$ at $p_L = 150$ and 280 GeV/c. The cross sections are reproduced to one standard deviation and, if corrected for different α_s used, they are 20—30 times larger than the perturbative QCD results. The differences between the calculated transverse differential cross sections for a single J/ψ and for the J/ψ pair and the experimental results are understandable in terms of the gluon transverse momentum. The calculated longitudinal differential cross section for a single J/ψ agrees qualitatively with the experimental data at $p_L = 280$ GeV/c, and less so with data at $p_L = 150$ GeV/c. The cross sections for the resonance production of $J\omega$, $D^*\bar{D}^*$, $J\phi$, $F^*\bar{F}^*$, $\Upsilon\Upsilon$, $\Upsilon\omega$, $B^*\bar{B}^*$, $\Upsilon\phi$, $B_s^*\bar{B}_s^*$, ΥJ, and $B_c^*\bar{B}_c^*$ are also calculated. They all grow with the energy; this is due to the small-x behavior of the gluon distribution functions.

ACKNOWLEDGMENT

*On leave from Institute of High Energy Physics, Beijing, China.

[1]J. Badier et al. (NA3 Collaboration), Phys. Lett. 114B, 457 (1982).

[2]R. E. Ecclestone and D. M. Scott, Phys. Lett. 120B, 237 (1983).

[3]V. Barger, F. Halzen, and W. Y. Keung, Phys. Lett. 119B, 453 (1982).

[4]Sh. M. Esakia and V. G. Kartvelishvili, Serpukhov report, 1983 (unpublished).

[5]B. Humpert and P. Méry, Phys. Lett. 124B, 265 (1983).

[6]B. A. Li and K. F. Liu, Phys. Rev D 28, 1636 (1983).

[7]T. Yamanouchi et al., Phys. Rev. D 23, 1514 (1981); D. R. Green, Fermilab Report No. 81/81-Exp (R) (unpublished); C.

Daum et al., Phys. Lett. 104B, 246 (1981).

[8]A. Etkin et al., Phys. Rev. Lett. 49, 1620 (1982).

[9]B. A. Li and K. F. Liu, Phys. Lett. 118B, 435 (1982); 124B, 550(E) (1983); B. A. Li and K. F. Liu, Phys. Rev. Lett. 51, 1510 (1983); N. N. Achasov et al., Phys. Lett. 108B, 134 (1982).

[10]TASSO Collaboration, R. Brandelik et al., Phys. Lett. 97B, 448 (1980); D. Burke et al., ibid. 103B, 153 (1982).

[11]D. L. Burke et al., Phys. Rev. Lett. 49, 632 (1982).

[12]J. G. McEwen et al., Phys. Lett. 121B, 198 (1983).

[13]H. Abramowitz et al., Z. Phys. C 12, 289 (1982).

[14]JADE Collaboration, W. Bartel et al., Phys. Lett. 123B, 460 (1983).